JOURNAL OF GUIDANCE, CONTROL, AND DYNAMICS
Vol. 23, No. 6, November–December 2000

Safety Constrained Free-Flyer Path Planning at the International Space Station

Alexander B. Roger* and Colin R. McInnes†
University of Glasgow, Glasgow, Scotland G12 8QQ, United Kingdom

A path-planning tool is presented to generate safe trajectories from an initial docking release, to a specified observation point, and back to docking for a small free-flying robot camera around the International Space Station. The tool makes use of ellipse of safety trajectories to enforce long-term passive safe requirements in the presence of differential air drag during the fly around phases of the maneuver during transfer between the docking port and observation point. Short-term passive safety (2–3 orbits) is also maintained during all station-keeping and approach maneuvers by checking the safety of the observation point at the initial planning stage, and through the use of precalculated velocities profiles along the r-bar forced motion approaches to the observation point and docking. The observation phase of the mission is enhanced through the use of artificial Laplace potential functions within a constrained volume, to allow for limited maneuvering close to the observation point enabling the available view to be translated and rotated.

Nomenclature

a	=	ellipse semimajor axis
b	=	ellipse semiminor axis
d	=	ellipse drift direction
f_x, f_y, f_z	=	externally applied forces on free flyer
G	=	universal gravitational constant
$K(x, y, z)$	=	laplace velocity profile
M	=	mass of Earth
m	=	free-flyer mass
r	=	International Space Station (ISS) orbital radius
$\boldsymbol{V}$	=	free-flyer velocity
x, y, z	=	free-flyer coordinates in ISS reference frame
$z_{\max}$	=	ellipse width
v_c	=	drift velocity of ellipse center
τ	=	maneuver transfer time
ϕ	=	Laplace potential
ω	=	orbital angular velocity
$\nabla\phi$	=	potential gradient

Subscripts

c	=	center of ellipse
d	=	required initial conditions
i, j, k	=	Laplace mesh node number
obs	=	observation point coordinates
t	=	Clohessy–Wiltshire maneuver target
x, y, z	=	component in x, y, and z direction
0	=	conditions at $t = 0$

I. Introduction

IN December 1998 the first two modules of the International Space Station (ISS), Unity and Zarya, were docked in orbit to complete the first step in the assembly of the new space station. As the ISS continues to grow into a large orbital facility, an external free-flying observation vehicle could provide desirable capabilities to document the latter stages of the assembly and record accurate reference information on the final ISS configuration. Once the station is operational, this vehicle could also enable various external observation and inspection tasks as well as possible maintenance and repair operations. Vehicles such as the DASA Inspector[1,2] and the NASA AERCam[3,4] are currently being developed to undertake some of these tasks.

To free astronauts onboard the ISS from some of the workload of controlling these free-flying vehicles, the vehicle operations could be enhanced through the use of autonomy, especially in such procedures as extended transfers from the initial docking release to a desired observation/inspection point for the mission and return to docking. However, due to the proximity of the vehicle to the crewed space station during these missions, the overriding requirement for path planning is that of safety.[5] Previous ESA/European Space Research and Technology Centre contract work at the University of Glasgow has developed a real-time controller for similar types of path constrained proximity operations.[6] This paper however, details the development of an offline path planning method, rather than a real-time controller, intended as an aid to mission planners, either on the ground or on the ISS. It is designed to be the first step in developing a tool to assist in quickly producing mission plans within the constraints of the observation and safety requirements for a range of mission applications. In addition to this, however, an active maneuvering phase of the mission may be used for real-time control, through precalculation of an artificial Laplace potential, which can then be uploaded to the free flyer for use by the vehicle for active guidance during constrained maneuvering at observation points.

A significant amount of work has already been done in the area of path planning, both offline and real time, using a number of different methods. One approach is to make use of potential functions.[7] These functions may be described analytically, as a potential field made of an attractive goal term and a series of repulsive terms used to represent obstacles, so that a path is found by descending through the potential field to reach the goal. The main difficulty with these types of potential functions is that because they are composed of multiple terms, local minima can be formed in the potential field, limiting the ability of the method to find paths to the desired goal. Alternatively, different types of artificial potential fields may be used,[8] modeled on equations such as an unsteady diffusion equation[9] and the Laplace equation.[10,11] Other methods include distance transform algorithms[12] and wave front methods.[13] Much of this previous work, however, has been applied to terrestrial mobile robots or robotic arms. Path planning for free-flying vehicles in the proximity of an orbital space structure, however, produces its own particular problems and requirements. These arise mainly from the orbital dynamics of the problem causing a free-flying vehicle to drift in

Received 10 June 1999; revision received 10 March 2000; accepted for publication 29 March 2000.

*Postgraduate Student, Department of Aerospace Engineering; aroger@aero.gla.ac.uk.

†Professor of Space Systems Engineering, Department of Aerospace Engineering; colinmc@aero.gla.ac.uk.

peculiar ways, the need to use impulse maneuvers and avoid forced motion to reduce propellant requirements, and the need for passive safety in case of system failure and free drift. For these reasons, potential function path planning will be used for close proximity maneuvering only and ellipse of safety (EOS) trajectories[14] used for the transfer to and from observation points. These types of maneuvers can be automatically evaluated to verify the safety of the trajectory, whereas for more complicated, less predictable paths, such as those generated by potential functions, this may not be possible.

II. Proximity Operations

Because the free-flying camera vehicle will be based at the ISS and all missions will take place within a maximum EOS orbit up to 500 m from the station, the vehicle maneuvers may be considered as proximity operations. Proximity operations are defined as maneuvers that take place within approximately 1–2 km of the origin of the reference coordinate system. This rotating coordinate system is fixed to the ISS, which is assumed to be in a circular orbit. In this case the local coordinate system is defined relative to the ISS, with the origin at the standard ISS reference point (at the ISS center of mass, near the center of the main truss), as shown in Fig. 1.

It is assumed that the axis system is orientated so that the x axis is aligned along the positive orbital velocity vector, the y axis is aligned along the outward radial direction, and the z axis completes the triad. The behavior of free-flying vehicles moving in such a rotating frame of reference can be described by a set of linearized equations, known as the Clohessy–Wiltshire (CW) equations,[15] the basic form of which are given by

$$\ddot{x} = -2\omega\dot{y} + (1/m)f_x \tag{1a}$$

$$\ddot{y} = 2\omega\dot{x} + 3\omega^2 y + (1/m)f_y \tag{1b}$$

$$\ddot{z} = -\omega^2 z + (1/m)f_z \tag{1c}$$

where ω is the orbital angular velocity of the reference system origin, given by

$$\omega = \sqrt{GM/r^3} \tag{2}$$

These equations of motion can then be rearranged and solved for the free-flyer position at time t given some initial position and velocity as

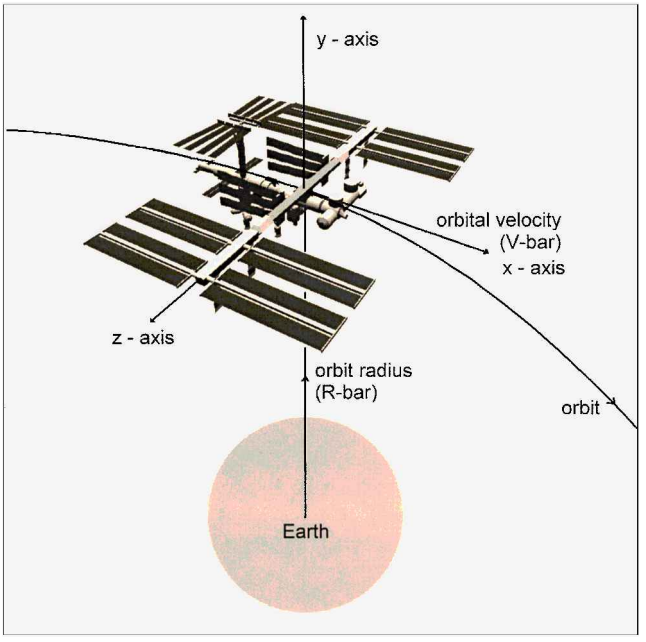

Fig. 1 Axis system at ISS reference point.

$$x(t) = x_0 - 6(\omega t - \sin\omega t)y_0 + [(4/\omega)\sin\omega t - 3t]\dot{x}_0 - (2/\omega)(1 - \cos\omega t)\dot{y}_0 + \left[(4/\omega^2)(1 - \cos\omega t) - \tfrac{3}{2}t^2\right] \times (1/m)f_x - [(2/\omega)t - (2/\omega^2)\sin\omega t](1/m)f_y \tag{3a}$$

$$y(t) = (4 - 3\cos\omega t)y_0 - (2/\omega)(\cos\omega t - 1)\dot{x}_0 + (1/\omega)\sin\omega t\,\dot{y}_0 - [(2/\omega^2)\sin\omega t - (2/\omega)t](1/m)f_x + (1/\omega^2)(1 - \cos\omega t)(1/m)f_y \tag{3b}$$

$$z(t) = z_0\cos\omega t + (\sin\omega t/\omega)\dot{z}_0 + (1/\omega^2)(1 - \cos\omega t)(1/m)f_z \tag{3c}$$

where it is assumed that the external forces are constant in magnitude. The free-flyer velocity at time t, given an initial position and velocity, is found to be

$$\dot{x}(t) = 6\omega(\cos\omega t - 1)y_0 + (4\cos\omega t - 3)\dot{x}_0 - 2\sin\omega t\,\dot{y}_0 + [(4/\omega)\sin\omega t - 3t](1/m)f_x - (2/\omega)(1 - \cos\omega t)(1/m)f_y \tag{4a}$$

$$\dot{y}(t) = 3\omega\sin\omega t\,y_0 + 2\sin\omega t\,\dot{x}_0 + \cos\omega t\,\dot{y}_0 - (2/\omega)(\cos\omega t - 1)(1/m)f_x + (1/\omega)\sin\omega t(1/m)f_y \tag{4b}$$

$$\dot{z}(t) = -\omega\sin\omega t\,z_0 + \cos\omega t\,\dot{z}_0 + (1/\omega)\sin\omega t(1/m)f_z \tag{4c}$$

By neglecting the external forcing terms, the CW equations can also be solved for the required initial velocity to pass through a target point, in a given transfer time τ. Letting $S_1 = \sin\omega t$, and $C_1 = \cos\omega t$, and defining

$$F_1 = 3\omega\tau S_1 + 8(C_1 - 1) \tag{5a}$$

$$F_2 = (y_0 - y_t)/(C_1 - 1) \tag{5b}$$

it is found that the required initial free-flyer velocities are given by

$$\dot{y}_{0_{\text{req}}} = (-\omega/F_1)(C_1 - 1)\{2(x_t - x_0) + 4F_2S_1 - 3\omega\tau(F_2 - y_0)\} \tag{5c}$$

$$\dot{x}_{0_{\text{req}}} = \frac{-\omega}{2}S_1\left\{3y_0 + F_2 + \frac{-\dot{y}_{0_{\text{req}}}}{\omega(C_1 - 1)}\right\} \tag{5d}$$

$$\dot{z}_{0_{\text{req}}} = (\omega/S_1)(z_t - z_0C_1) \tag{5e}$$

where the subscript t denotes the target conditions of the maneuver, and 0_{req} denotes the required initial velocities to reach the target.

III. Ellipse of Safety Trajectories

EOS trajectories are designed so that the free-flyer path describes an ellipse around the origin in both the orbital plane (x–y plane), and the plane with normal along the v-bar axis (y–z plane) as shown in Figs. 2a and 2b. This is achieved by first setting up an ellipse orbiting the origin in the x–y plane and then making an out-of-plane burn to increase the inclination of the ellipse to the ISS orbital plane at the apogee or perigee. This maneuver is performed so that as the in-plane motion crosses the x axis ($y = 0$) the out-of-plane position is at a maximum $z = z_{\max}$, as shown in Fig. 2b.

The aim of this strategy is to guard against the long-term effects of differential air drag in the event of propulsion failure. Because the drag force will always act opposite to the free-flyer velocity, the effect over time will be that the in-plane ellipse will slowly drift forward or back along the v bar, depending on the differential drag between the ISS and the free-flying camera. However, because the out-of-plane motion is uncoupled from this, and there is no force acting in the z axis, the inclination of the ellipse will remain constant. In the presence of differential air drag, the free-flyer will, therefore, describe a helical spiral about the ISS, as shown in Fig. 2c.

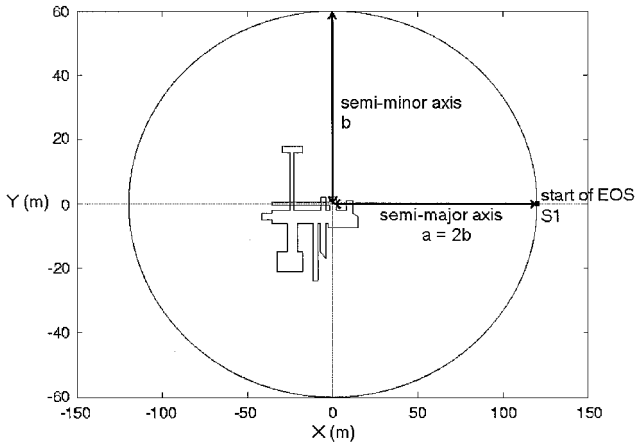

a) In-plane motion (no differential drag)

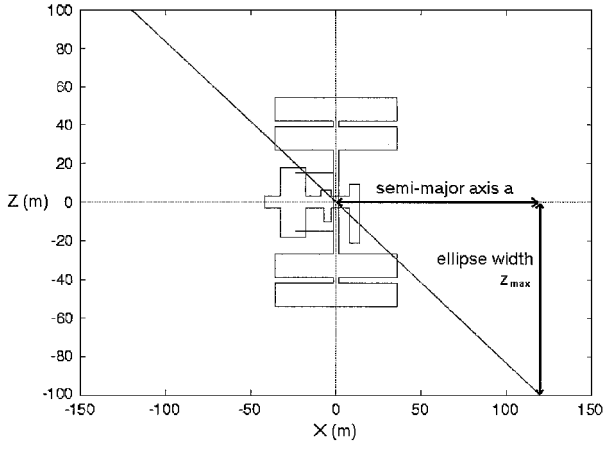

b) Out-of-plane motion (x–z plane, no differential drag)

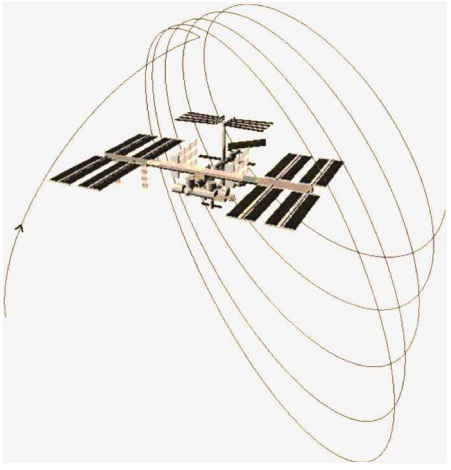

c) Spiral motion due to air drag

Fig. 2 Example EOS trajectories.

To evaluate these ellipse trajectories, it is useful to rearrange the solutions of the CW equations to describe the motion on the ellipse by parameters independent of time. Equations (3a) and (3b) describe the in-plane motion of a drifting ellipse, whose dimensions are elongated such that its semimajor axis a is twice the size of its semiminor axis b, and whose center remains at a constant altitude with respect to the orbital frame of reference and drifts in the x direction with a velocity of

$$v_c = -3(\dot{x}_0 + 2\omega \cdot y_0) \tag{6}$$

From Eqs. (3a) and (3b), the center of the ellipse can be obtained by eliminating the periodic terms and neglecting the external forcing terms, to get

$$x_c = x_0 - 2\dot{y}_0/\omega \tag{7a}$$

$$y_c = 4y_0 + 2\dot{x}_0/\omega \tag{7b}$$

We can then express positions on the ellipse, for example, x_0, y_0, relative to the ellipse center position as

$$\alpha = x_0 - x_c = 2\dot{y}_0/\omega \tag{8a}$$

$$\beta = y_0 - y_c = -3y_0 - 2\dot{x}_0/\omega \tag{8b}$$

Because of the 2×1 dimensions of the ellipse, the semiminor axis b can, therefore, be obtained from any ellipse position (α, β), by

$$b = \sqrt{\beta^2 + (\alpha/2)^2} = \sqrt{(\dot{y}_0/\omega)^2 + [3y_0 + 2(\dot{x}_0/\omega)]^2} \tag{9}$$

This gives the semimajor axis $a = 2b$.

The out-of-plane motion of the EOS is most easily described by the maximum out-of-plane position on the ellipse. This is termed the ellipse width $z_{\max}$, and is obtained from Eq. (3c), solving for $z = z_{\max}$, to get

$$z_{\max} = \sqrt{z_0^2 + (\dot{z}_0/\omega)^2} \tag{10}$$

It is clear now that for a given set of initial conditions the size and shape of the EOS can be selected.

IV. Camera Simulation

The initial stage of planning any observation or inspection mission must be to find a suitable position for the camera to provide the optimum view of the target. In addition, the camera position must provide good radio coverage from the available antenna on the ISS for S-band video broadcast and must be passively safe in case of a propulsion failure during station keeping. These are not easy constraints to satisfy analytically due to the high complexity of the ISS structure, as well as the counterintuitive nature of the orbital dynamics. A graphical model of the ISS has, therefore, been developed to aid in the selection of viewing positions. The camera simulation tool provides a virtual view through the camera lens, as can been seen in Fig. 3a, while at the same time determining passive free-drift safety and line-of-sight radio contact at the camera position. In addition, it also provides an external view of the ISS and the free-flying camera, including the camera field of view, to aid the operator in visualizing the spatial orientation of the vehicle with respect to the ISS, thus aiding the selection of more easily accessible viewing positions, as shown in Fig. 3b.

The camera simulation tool is first given an initial camera position and viewing target position based on the desired mission. The virtual camera can then be zoomed in and out, translated in space while tracking the target point, or rotated around a fixed position to allow the operator to choose the best observation coordinates to fulfill all of the mission requirements. As the camera position is translated, the simulation continually recalculates passive station-keeping safety of the current location by propagating the free-drift path for a number of orbits and checking for possible collisions. In addition, the simulation also checks the radio coverage both for the S-band video transmission and for the longer wavelength command and telemetry link. This is achieved by checking for intersections between the line of sight from the camera to the antenna [which in the test case is situated on the Columbus Orbital Facility (COF) module] and the ISS structure. This information is displayed on the camera simulation window (Fig. 3a) as three icons, representing the integrity of the communications radio link, the video transmission signal, and the station-keeping safety.

V. Mission Overview

Once the observation coordinates have been defined, the task of planning the required maneuvers to reach this goal begins. The mission as a whole can be divided up into the following three distinct phases, shown in Fig. 4:

1) Phase 1 involves free-drift retreat with initial downward pushoff from docking, maneuver onto EOS transfer trajectory to pass over/below observation coordinates (x_{obs}, y_{obs}, and z_{obs}), and forced motion along the r-bar axis to reach the observation coordinates.

2) Phase 2 involves station keeping during observation, and constrained maneuvering using artificial Laplace potentials to enhance imaging.

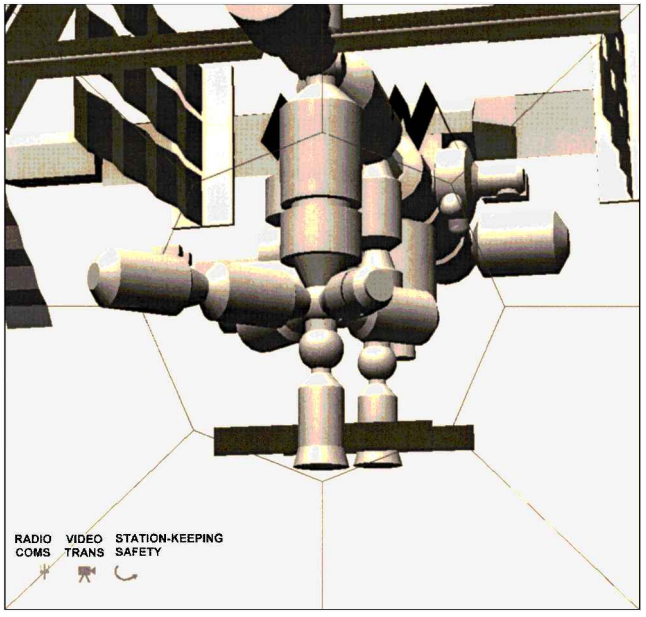

a) Virtual view through camera lens

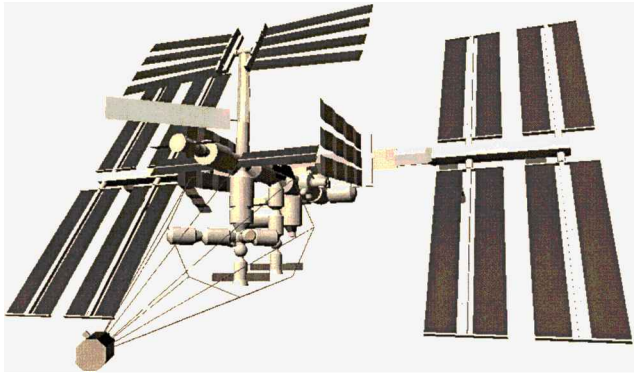

b) External view of free flyer and ISS

Fig. 3 Example camera simulation views.

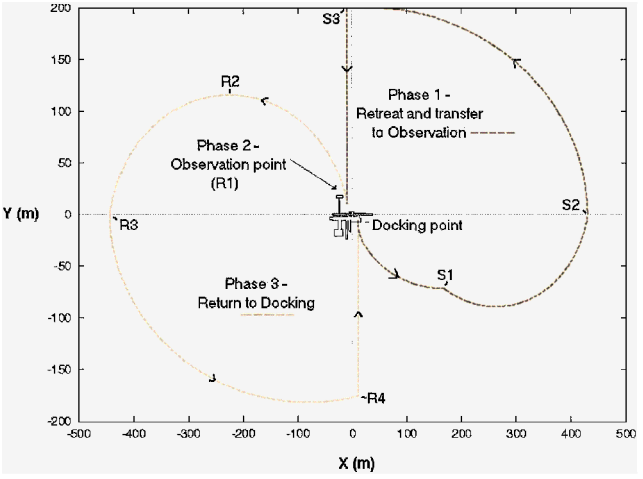

Fig. 4 Complete mission trajectory in orbital plane.

3) Phase 3 involves a single impulse to start free-drift retreat from observation position, maneuvers to attain desired EOS trajectory to pass under docking port (on COF), and forced motion up the r-bar axis to berthing.

The planning of the approach and retreat phases of the mission is made by adjusting a predefined sequence of maneuvers to set up the EOS trajectories and to make sure they pass over/under the desired observation coordinates and docking port. In the case of the transfer to the observation point, this is achieved by moving the entire EOS trajectory along the x axis and, for the return to docking, by varying the timing of the initial maneuvers to control phasing between the out-of-plane and in-plane motion and, hence, varying the path of the EOS trajectory to pass under the docking port. The observation phase is less constrained in the type of paths that may be produced because the maneuvers will only be determined as the path is being found through the Laplace potential field and trajectory changes are made as necessary. This phase is, however, constrained in the volume of space within which it may maneuver to increase the safety of the paths found. Phase 2 and the use of potential functions will be described later in Sec. VIII.

VI. Phase 1, Transfer to Observation Point

The transfer from initial docking release to the observation point comprises three main elements: 1) pushoff from docking and free drift away from the ISS followed by maneuvers at S_1 to set the EOS inclination and reach the EOS start point S_2, as shown in Fig. 4; 2) injection onto the desired EOS trajectory at S_2, which crosses the desired observation point at S_3; and 3) forced motion up or down the r bar from S_3 to reach the observation point.

The first step in planning this phase of the mission is to choose an appropriate EOS trajectory that will pass across the desired observation point coordinates in the x–z plane. To simplify the analysis and maintain required clearances around the ISS, this is achieved by fixing the dimensions of the ellipse and then choosing the position of the S_2 point along the x axis to shift the whole ellipse forward and back, so that it crosses the desired position.

The EOS dimensions are defined by the requirements imposed on certain operational parameters. Navigational requirements show that to enable the vehicle to receive accurate relative global positioning system positioning information, the vehicle should be at least 200 m from the station to avoid interference.[5] Because the ellipse size b of the EOS gives the closest distance from the path to the ellipse center, and, hence, the closest approach to the ISS during the EOS transfer, the ellipse size is set to 200 m. With the ellipse size defined, the ellipse width z_{max} is then chosen to ensure a safe margin around the ISS in the y–z plane. This should be valid for any station configuration and so is calculated for the worse case where the solar panels are orientated at 90 deg to the x–z plane, that is, perpendicular to the x axis. However, increasing the ellipse width has a drastic effect on propellant requirements, and so it should not be made any greater than necessary. For an ellipse size of 200 m, an ellipse width of 100 m is sufficient to ensure safety for the EOS phase of the maneuver.

The method used to calculate the desired ellipse start point S_2 is to look at the ellipse motion in the x–z plane. The desired goal point is projected across to the ellipse width, at an angle defined by the ratio of z_{max}/a, giving the x coordinate at this point as the S_2 position. However, the method must account for starting positions on both sides of the x axis. The easiest way to achieve this is to shift the coordinates to the positive z axis side by adding the ellipse width z_{max} to the starting z coordinate, before projecting back to the x axis by dividing by the ratio z_{max}/a, and finally adding the start x coordinate:

$$S_2 = x_{obs} + (a/z_{max})(z_{max} + z_{obs}) \tag{11}$$

This gives the start point for an ellipse inclined so that ahead of the station it passes to the left side and crosses to the right side at the rear. However, some areas of the ISS, such as the forward right or rear left solar panels, will not be easily reachable without shifting the ellipse far back in relation to the station. In this case, the inclination is reversed by the selection routine to keep the ellipse better

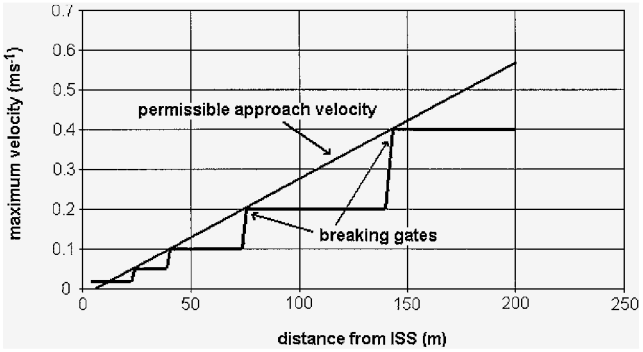

Fig. 5 Approach braking velocity profile.

centred around the ISS by projecting the goal point in the opposite direction:

$$S_2 = x_{\text{obs}} + (a/z_{\max})(z_{\max} - z_{\text{obs}}) \tag{12}$$

The vehicle is released from docking at the COF with a downward velocity of 0.05 m s^{-1} and allowed to drift for approximately half an orbit to perigee (S_1) while the in-flight systems checks are carried out. This is safe because of the position of the COF below the center of mass of the ISS and, hence, below the v bar, because unchecked the free-drift trajectory from release will continue on a drifting ellipse ahead of the station. In the case that the ISS is oriented in its torque equilibrium attitude, the COF would be even farther below the v bar, however, if the docking position was moved to above the v bar the release strategy would have to be changed to ensure safety.

The path from docking release is calculated using the CW equations of motion, solving the y-velocity equation, Eq. (4b), for $\dot{y}(t) = 0$ to get the S_1 point where the path reaches perigee (bottom of the ellipse). This will be approximately one-quarter orbit since release, though slightly less due to the initial downward velocity. At S_1 two burns are made, an in-plane burn to reach the desired S_2 coordinates in a specified transfer time of one-quarter orbit, and an out-of-plane burn to set the ellipse widht to $z_{\max}$. The required initial velocities for these maneuvers are calculated using the targeted form of the CW equations as given in Eqs. (5a–5e). The transfer time of one-quarter orbit is selected because this will help phase the in-plane and out-of-plane motions once the S_2 position is reached and should also result in the in-plane velocity at S_1 being in the correct direction required for the EOS trajectory, thereby helping to reduce propellant requirements.

At S_2 the path must be set onto the defined EOS. Because the maneuver is taking place at $y = 0$, from EOS Eq. (6) it can be seen that the x velocity must be zero, and so Eq. (9) reduces to

$$b = \dot{y}_0/\omega \Rightarrow \dot{y}_0 = b\omega \tag{13}$$

As the EOS trajectory passes over (or under) the observation coordinates at the S_3 point, the free-flyer velocity on the EOS is removed, and the path begins a forced motion approach to the goal along the r bar. This maneuver is managed using the developed ISS Inspector r-bar approach.[16] The velocity in the y axis is selected such that in case of propulsion failure, the free-drift trajectory cannot reach the ISS, and so the closer the approach, the smaller the maximum allowable velocity will be. This is achieved through the use of braking gates during the path, which are precalculated to ensure passive safety (see Fig. 5), and through the use of the camera simulation tool when selecting the observation points because this automatically checks the free-drift safety at the goal, thereby precluding the selection of any unreachable points.

VII. Phase 3, Retreat and Return to Docking

The strategy for planning the return to docking is slightly different from the transfer to the observation point because the starting position of the maneuver is not known, whereas the goal coordinates are. Thus, rather than a sequence of maneuvers from a standard starting position to move to the desired EOS, there is a sequence of maneuvers from an arbitrary start point, designed to get to a fixed EOS to reach the standard docking position. This phase can also be broken up into four main sections: 1) move to safe retreat point R_1 using Laplace potentials as in phase 2, 2) retreat from observation point R_1 with an impulse maneuver, 3) EOS transfer around ISS to pass under docking port, and 4) forced motion from R_4 up the r bar to docking.

The desired first maneuver of the return phase is the retreat from the observation point. For most cases this will be performed through a single impulse to inject the vehicle onto a safe ellipse drifting away from the ISS. In certain cases, however [e.g., for observation positions close to the x axis and in front of the science power platform (SPP) core and photo voltaic array], an additional maneuver is required to clear the ISS structure before the impulse maneuver may be safely performed. A safety envelope is, therefore, calculated to determine which areas around the ISS are unsafe for a single impulse retreat, so that the path planner can use Laplace potential maneuvering to retreat to a point outside this envelope, before initializing the retreat impulse.

The drift trajectory retreat maneuver itself is designed so that the ellipse semiminor axis b is the same as that of the standard EOS (as in phase 1), except that the ellipse center will drift along the x axis at a rate of $4b$ meters per orbit. This drift rate is required to ensure that the ISS will be outside of the ellipse at the end of the first orbit, thus maintaining passive safety should a problem occur before the inclination can be set up. A maneuver can then be made at R_3 to remove the drift and enter the desired EOS trajectory, and if the planned maneuver at R_2 or R_3 fails for any reason, the ellipse drift will ensure that the subsequent path will avoid the ISS and will continue to drift safely away from the station.

In addition, a small out-of-plane impulse is made at R_1 to ensure that the z motion crosses the orbital plane at the desired point R_2. This is necessary to compensate for any initial out-of-plane offset at the observation point, which would cause out-of-plane periodic motion not necessarily in phase with the desired in-plane motion. At R_2 the z coordinate should, therefore, be zero, and here the main out-of-plane maneuver is made to increase the EOS width to $z_{\max}$ as in phase 1. The R_2 point, however, will not necessarily be exactly at the apogee of the ellipse, as would normally be required to correctly phase the in-plane and out-of-plane motion. The path planner intentionally uses a slight deviation between the phasing, causing the ellipse to tilt about its major axis, to adjust the ellipse path to cross under the docking port with varying ellipse start points.

The second in-plane impulse is made at R_3 as the free flyer crosses the x axis. This has the objective of removing the drift velocity from the ellipse by making a burn in the x axis, while leaving the y velocity unchanged. It is safe to remove the drift from the EOS at this point because the ellipse inclination has now been set up, ensuring the passive safety of the ellipse.

As the EOS passes under the docking point at R_4, the ellipse velocity is removed, and the vehicle then uses a forced motion approach up the r bar, as described in phase 1. The velocity profile used in unchanged since it was calculated for approach to an observation point above or below the ISS.

The calculation of the required ΔV, and especially the timing for phase 3, is also significantly different from that of phase 1. To determine the timing for the out-of-plane burn at R_2 and control the phasing with the in-plane motion so that the target point is crossed, the complete in-plane path must be calculated first, and then the out-of-plane motion must be calculated in reverse to work back to the R_2 time. The sequence of these calculations is detailed in Table 1.

First of all, the retreat safety envelope must be checked and a forced motion maneuver performed if required. In most cases, however, this should not be necessary. The initial in-plane ΔV is then calculated using the EOS equations for a drifting ellipse of size $b = 200$ m and a drift velocity in the x axis $v_c = 4bd$, where d is the drift direction. For observation coordinates above the ISS, d is set to -1 so the path will drift off behind the station, whereas for observation points below the station, d is set to $+1$.

Once the free-drift retreat maneuver has been calculated, the path is then propagated using the CW equations, Eqs. (3a–3c), until it crosses the x axis ($y = 0$), giving the time and position of the R_3

Table 1 Calculation sequence for return trajectory (phase 3)

Calculation type	Position in maneuver	Aim of calculation
ΔV: in-plane	R_1	Set up 200-m EOS with V_c = 4ed
Propagate path (in-plane)	R_1–R_3	Get time at point R_3
ΔV: in-plane, x axis only	R_3	Remove ellipse drift
Propagate path (in-plane)	R_3–R_4	Get time at point R_4
ΔV: out-of-plane	R_2	Set EOS width to Z_{max} starting at R_2 (where z = 0, time unknown)
Propagate path[a] (out-of-plane)	R_2–R_4	Calculate time from R_2 to R_4 due to out-of-plane motion
Calculate time	R_2	Get time at R_2 from known time at R_4
ΔV: out-of-plane	R_1	Get initial impulse required to get z = 0 at R_2 from initial z position

[a]Get time from R_2 to R_4 within correct interval: When $y(R_1/R_2) \geq 0$, $R_3 \rightarrow R_4$ time = 0–$\frac{1}{2}$ orbit and $R_2 \rightarrow R_4$ time = $\frac{1}{4}$–$\frac{3}{4}$ orbit. When $y(R_1/R_2) < 0$, $R_3 \rightarrow R_4$ time = $\frac{1}{2}$–1 orbit and $R_2 \rightarrow R_4$ time = $\frac{3}{4}$–1$\frac{1}{4}$ orbit.

point. At R_3 the maneuver to enter the EOS trajectory by removing the ellipse drift must be made. This is calculated by determining the x velocity required for a zero drift ellipse at the R_3 coordinates from Eq. (6) and setting the y velocity to the current value at R_3. The path is then propagated again until the in-plane motion crosses under the docking port, giving the time and position at R_4.

With the in-plane motion calculated, the timing for the R_3 and R_4 points can then be used to determine the required timing for R_2 and, hence, the calculation of the out-of-plane motion. The first step is to calculate the z velocity that will be required at R_2 to attain the desired ellipse width z_{max}. The out-of-plane motion can then be propagated from this point, to determine the time interval after R_2 when it will reach the docking z coordinate, given z_{max}. However, it must be ensured that the correct root is found when solving the out-of-plane motion equation (3c) for $z = z_{docking}$ because it may be that the out-of-plane coordinate also crosses the goal z coordinate while the in-plane motion is in a different section of the ellipse. The z coordinate is, therefore, only searched for within a certain desired time period to limit the possible solutions, as shown in Table 1. It can be shown that for R_2 points above the x axis ($y > 0$), the path should pass under the docking port within one-half orbit from the x-axis crossing, or between one-quarter and three-quarter orbits from the R_2 point. For starting points below the ISS, the path should pass under the goal between one-half and one orbit from the first x axis crossing, or from three-quarter to five-fourth orbits from R_2 because the path must cross completely above the station before passing back under. Now, because the time at R_4 is known from the in-plane calculations, and the time from R_2 to R_4 has just been calculated, the time at R_2 can be determined by subtracting the two. The final maneuver to be calculated is then the initial out-of-plane ΔV to make sure that the z position at R_2 is zero given any initial out-of-plane coordinate at the observation point. This can be simply done by using the targeted CW equations to reach $z = 0$ in the calculated time to R_2.

VIII. Phase 2, Laplace Artificial Potential Guidance

For the observation phase of the mission, limited maneuvering within a constrained volume surrounding the observation points is desired. There are, however, a number of problems involved in maneuvering in arbitrary directions within such close proximity to the ISS. The most important of these from a safety point of view is that it is not possible to ensure that passive trajectories are always used because this would greatly limit the areas that could be reached and, hence, limit the benefits of maneuvering in phase 2. The risks of travelling on these nonpassively safe trajectories may be reduced, however, by first of all ensuring the fault tolerance of the vehicle systems.[17] Also, because certain impact loads are already anticipated and planned for the ISS structure to allow for kickoff loads applied by astronauts (of similar mass to the planned Inspector free flyer) when performing extravehicular activity missions, if the free-flyer vehicle velocities can be limited so that any possible impact would be within these expected loads, then catastrophic impacts may be avoided. The actual path planning and guidance within the desired maneuvering space is achieved by generating an artificial Laplace potential field ϕ between the volume boundary walls and the obstruction walls, which all have the maximum potential value of 1 and the desired goal point that is assigned a value of 0. The obstructions are due to the elements of the ISS structure, which protrude into the volume in which the free flyer will maneuver. The Laplace potential field is calculated by finding a solution to Laplace's equation within the control space

$$\nabla \cdot (\nabla \phi) = \frac{\partial^2 \phi}{\partial x^2} + \frac{\partial^2 \phi}{\partial y^2} + \frac{\partial^2 \phi}{\partial z^2} = 0 \tag{14}$$

If Eq. (14) is satisfied, then the potential function ϕ is, therefore, a harmonic function, and hence, it can have no local minima. This is extremely useful because it means that a path will always be found (if one exists) to the one minimum in the potential field, at the goal.

It is not possible to solve the Laplace equation for this volume analytically, and so a discrete numerical method must be used. The obstacles and surrounding space are divided up into a mesh grid, and a discrete form of the Laplace equation is applied iteratively. The Laplace differential equation [Eq. (14)] can be replaced by the difference equation

$$\begin{aligned} 0 = {} & \frac{1}{\Delta x}\left(\frac{\phi_{i+1,j,k} - \phi_{i,j,k}}{\Delta x} - \frac{\phi_{i,j,k} - \phi_{i-1,j,k}}{\Delta x}\right) \\ & + \frac{1}{\Delta y}\left(\frac{\phi_{i,j+1,k} - \phi_{i,j,k}}{\Delta y} - \frac{\phi_{i,j,k} - \phi_{i,j-1,k}}{\Delta y}\right) \\ & + \frac{1}{\Delta z}\left(\frac{\phi_{i,j,k+1} - \phi_{i,j,k}}{\Delta z} - \frac{\phi_{i,j,k} - \phi_{i,j,k-1}}{\Delta z}\right) \end{aligned} \tag{15}$$

where Δx, Δy, and Δz are the step sizes between mesh points in each direction. If the grid is equally spaced, that is, the step size are equal, Eq. (15) can be written as

$$\begin{aligned} & \phi_{i+1,j,k} + \phi_{i-1,j,k} + \phi_{i,j+1,k} + \phi_{i,j-1,k} + \phi_{1,j,k+1} \\ & \quad + \phi_{i,j,k-1} - 6\phi_{i,j,k} = 0 \end{aligned} \tag{16}$$

or

$$\begin{aligned} \phi_{i,j,k} = {} & \tfrac{1}{6}\{\phi_{i+1,j,k} + \phi_{i-1,j,k} + \phi_{i,j+1,k} \\ & + \phi_{i,j-1,k} + \phi_{i,j,k+1} + \phi_{i,j,k-1}\} \end{aligned} \tag{17}$$

The initial value of the potential ϕ at each point is set to a value of 1, and the potential at the specified goal set to 0. The value of the potential at any node on the mesh that is defined as a boundary point is then fixed so that the boundary potentials will remain at 1 during the iterations, whereas the free-space potentials will change. The goal potential is also fixed, to remain at 0. The calculations for the discrete Laplace potential over the control volume are then carried out by iteratively applying Eq. (17) at each of the nonfixed nodes.

The use of an initial potential value of 1 at all of the nodes means that as the iterations progress, the lower potential value at the goal gradually propagates out around the surrounding obstacles. This can be more easily visualized in two dimensions as can be seen in Fig. 6. The discrete potential values calculated at the nodal points may then

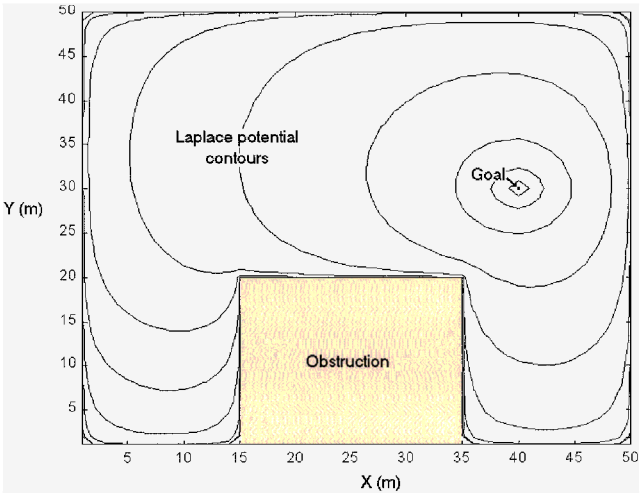

Fig. 6 Laplace artificial potential field.

be linearly interpolated[18] between the surrounding nodes to obtain the potential at any point within the control space as

$$\begin{aligned}\phi(x,y,z)_{i,j,k} &= \phi_{i,j,k}\cdot(i+1-x)(j+1-y)(k+1-z)\\ &+\phi_{i+1,j,k}\cdot(x-i)(j+1-y)(k+1-z)\\ &+\phi_{i,j+1,k}\cdot(i+1-x)(y-j)(k+1-z)\\ &+\phi_{i+1,j+1,k}\cdot(x-i)(y-j)(k+1-z)\\ &+\phi_{i,j,k+1}\cdot(i+1-x)(j+1-y)(z-k)\\ &+\phi_{i+1,j,k+1}\cdot(x-i)(j+1-y)(z-k)\\ &+\phi_{i,j+1,k+1}\cdot(i+1-x)(y-j)(z-k)\\ &+\phi_{i+1,j+1,k+1}\cdot(x-i)(y-j)(z-k)\end{aligned}\tag{18}$$

where $\phi(x,y,z)_{i,j,k}$ is the Laplace potential value at coordinate (x,y,z) that lies within the mesh cell (i,j,k).

By differentiating this interpolation equation with respect to x, y, and z, we can then interpolate the potential gradient in each of the three axial directions from the nodal potentials

$$\begin{aligned}\frac{\partial\phi}{\partial x} &= \phi_{i,j,k}\cdot(y-j-1)(k+1-z)\\ &+\phi_{i+1,j,k}\cdot(j+1-y)(k+1-z)\\ &+\phi_{i,j+1,k}\cdot(j-y)(k+1-z)\\ &+\phi_{i+1,j+1,k}\cdot(y-j)(k+1-z)\\ &+\phi_{i,j,k+1}\cdot(y-j-1)(z-k)\\ &+\phi_{i+1,j,k+1}\cdot(j+1-y)(z-k)\\ &+\phi_{i,j+1,k+1}\cdot(j-y)(z-k)\\ &+\phi_{i+1,j+1,k+1}\cdot(y-j)(z-k)\end{aligned}\tag{19a}$$

$$\begin{aligned}\frac{\partial\phi}{\partial y} &= \phi_{i,j,k}\cdot(x-i-1)(k+1-z)\\ &+\phi_{i+1,j,k}\cdot(i-x)(k+1-z)\\ &+\phi_{i,j+1,k}\cdot(i+1-x)(k+1-z)\\ &+\phi_{i+1,j+1,k}\cdot(x-i)(k+1-z)\\ &+\phi_{i,j,k+1}\cdot(x-i-1)(z-k)\\ &+\phi_{i+1,j,k+1}\cdot(i-x)(z-k)\\ &+\phi_{i,j+1,k+1}\cdot(i+1-x)(z-k)\\ &+\phi_{i+1,j+1,k+1}\cdot(x-i)(z-k)\end{aligned}\tag{19b}$$

$$\begin{aligned}\frac{\partial\phi}{\partial z} &= \phi_{i,j,k}\cdot(i+1-x)(j+1-y)\\ &+\phi_{i+1,j,k}\cdot(x-i)(j+1-y)\\ &+\phi_{i,j+1,k}\cdot(i+1-x)(y-j)\\ &+\phi_{i+1,j+1,k}\cdot(x-i)(y-j)\\ &+\phi_{i,j,k+1}\cdot(x-i-1)(j+1-y)\\ &+\phi_{i+1,j,k+1}\cdot(i-x)(j+1-y)\\ &+\phi_{i,j+1,k+1}\cdot(x-i-1)(y-j)\\ &+\phi_{i+1,j+1,k+1}\cdot(i-x)(y-j)\end{aligned}\tag{19c}$$

To find a path through the potential field to the goal, the orbital mechanics of the problem must also be taken into account. The guidance scheme used here attempts to make use of the characteristics of free-drift trajectories wherever possible, by allowing the path to drift freely as long as the change in potential remains negative, that is, the path is always moving down the potential gradient. When the rate of change of the potential becomes positive, an impulse is made in the direction of steepest descent of the potential and the path is allowed to drift again using

$$\boldsymbol{V}+\Delta\boldsymbol{V}=-K(x,y,z)(\nabla\phi/|\nabla\phi|)\qquad\text{if}\qquad\dot{\phi}\geq 0\tag{20}$$

where $K(x,y,z)$ represents the desired velocity profile, which may be shaped to vary the free-flyer speed depending on its range to the ISS, and $\nabla\phi$ is the potential gradient given in component form by

$$\nabla\phi=\frac{\partial\phi}{\partial x}\boldsymbol{i}+\frac{\partial\phi}{\partial y}\boldsymbol{j}+\frac{\partial\phi}{\partial z}\boldsymbol{k}\tag{21}$$

This behavior can be seen in Fig. 7, which shows the path that is followed using the free-drift trajectories with control impulses when required. Each of the discontinuities in the smooth path show where a control action has taken place, with the path direction directly after the ΔV impulse indicating the direction of steepest descent $\Delta\phi$ through the potential field at that point.

The advantages of the Laplace method are that it can be formulated (as described) to guarantee the avoidance of local minima so that a path will always be found to the goal. It produces smooth paths through complicated fields of obstacles and ensures safe clearance between obstacles due to the averaging effect of the Laplace equation. Complex obstacles such as the ISS can be easily represented. It is also possible to have goal points close to boundary wall, for example, for future repair missions.

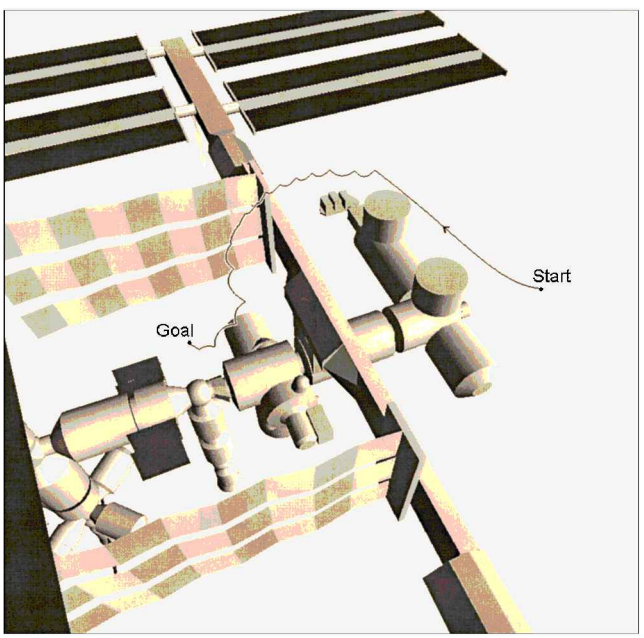

Fig. 7 Example Laplace path implementing orbital dynamics and control laws.

The main disadvantage, however, is in the amount of computation required to calculate the iterations of the discrete Laplace equation for each mesh point and that any change in boundary conditions, or in the goal point, requires a complete recalculation of the potential field. This method is not, therefore, suited to situations involving moving or unexpected obstacles, although the possibility of using a compound potential by adding a simple additional term for an unexpected boundary condition to provide safety may be considered. The computational problem is partly helped through the planned use of a small constrained volume around the desired start/goal coordinates so that the control volume and, hence, the mesh size is considerably reduced compared to the size of the entire ISS. Also, because all of these computational requirements will be carried out prior to the mission and should be performed by computing facilities on the ground or ISS where processing power is not an issue, the calculation required for the Laplace method is not seen as a significant problem.

IX. Results

The path-planning methods presented have been tested for a large number of varied observation positions and transfers around the ISS to produce a wide range of mission profiles, such as those detailed in Table 2 and illustrated in Figs. 8 and 9.

The first two example trajectories in Table 2 show transfers to observation points above the ISS. In these cases, the vehicle performs approximately one-half an EOS orbit to reach the hold point above the observation point at S_3, and one-half an orbit to transfer back to below the docking port at R_4. In contrast, the second two examples show the results of transfers to observation points below the station, take around three-quarter to one orbit to pass under the goal coordinates, and take another complete orbit to return to below the docking position, as shown in Fig. 8. This gives an effective range for the transfer time of 2–3 complete orbits between the best and worse case scenarios. It can also be seen, however, that the variation in goal point location has little impact on the ΔV requirement for the transfer. This is due to the free drift of the EOS trajectories, which does not use any fuel once the ellipse has been initiated.

Two examples of constrained maneuvering from the observation point are shown in Figs. 9a and 9b. The rectangular box represents the volume within which the Laplace potentials are calculated, and the small dots on the ISS show the boundary points that are defined to represent the obstructions caused by the ISS within this volume and

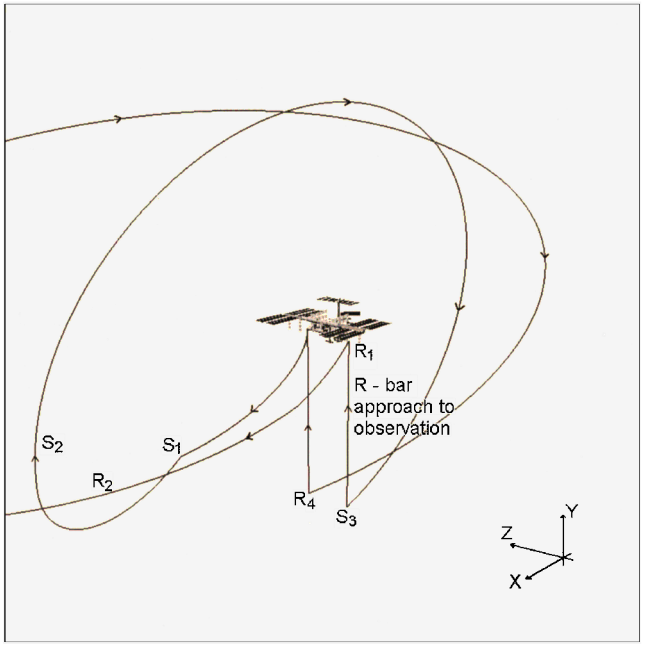

Fig. 8 Example result from phases 1 and 3, transfer and return to observation below and to the port side of the ISS.

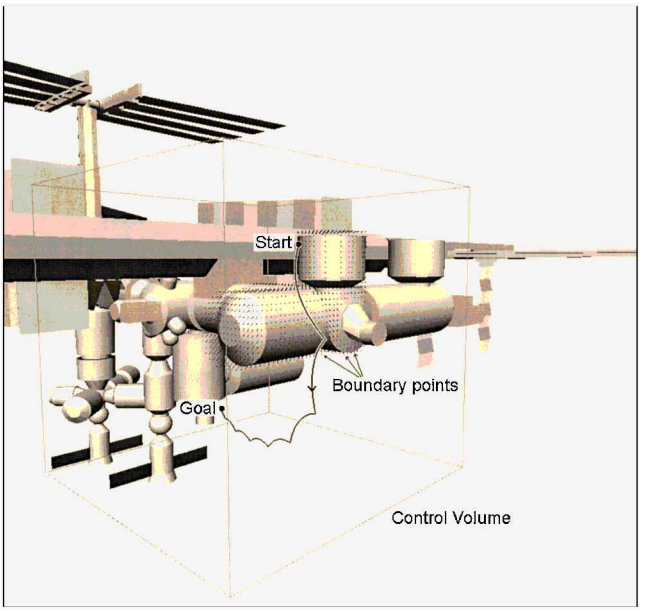

a) Inspection around the COF module from above to below

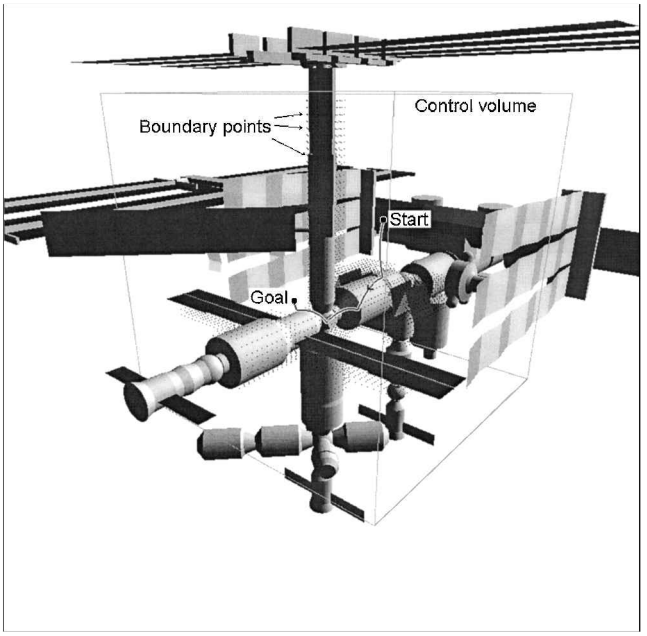

b) Maneuver to the rear of the ISS from ahead of the SPP core

Fig. 9 Results of phase 2 Laplace maneuvers.

Table 2 Numerical results from test cases

Example number	Transfer type	Start point coordinates	Goal point coordinates	Total transfer time	ΔV required, m/s
A	EOS	(10, −6, 10) docked	(−6, 10, 15)	11,969	1.875
B	EOS	(10, −6, 10) docked	(−36, 5, 0)	12,187	1.859
C (Fig. 8)	EOS	(10, −6, 10) docked	(−16, −18, −20)	16,777	1.815
D	EOS	(10, −6, 10) docked	(0, −7, 35)	16,818	1.876
E (Fig. 9a)	Laplace	(15, 0, 7)	(8, −10, 7)	1,922	0.1261
F (Fig. 9b)	Laplace	(−15, 3, 0)	(−28, 0, 3)	2,143	0.0639

that are used to calculate the discrete Laplace potential. The free-drift characteristics are clearly visible between each of the control maneuvers, where a burn is made to ensure the potential is decreasing. Figure 9a shows a trajectory from in front and above the COF to below the module, demonstrating how maneuvers may be used to inspect around an ISS element. The use of Laplace maneuvering to reach normally inaccessible observation points can be seen in Fig. 9b because the goal position to the rear of the SPP core would not normally be reachable through a forced motion approach down the r bar.

X. Conclusion

The results obtained from the path-planning methods have demonstrated the ability of EOS trajectories to safely reach most desired observation points around the ISS and to return to the docking point while ensuring passive safe trajectories throughout the transfer. This is an important step in moving toward the goal of having free-flying vehicles operating in close proximity to a crewed space station. In addition, it has been shown that the Laplace artificial potential guidance method brings significant enhancements to the mission, allowing observations from points that would not otherwise be accessible and providing the ability to inspect objects from different angles and positions during the same mission. The results of the Laplace method have demonstrated the technique's ability to reliably generate trajectories around complex structures such as the ISS, while ensuring that the goal point may be reached. The Laplace method does not, however, at this point ensure the free-drift safety of these trajectories, though this may be implemented through the use of velocity shaping at the impulses and possible collision dangers constrained to noncatastrophic collisions such as those already envisaged from astronaut kickoff loads.

Acknowledgments

This research has been funded by the Engineering and Physical Sciences Research Council, through the University of Glasgow. We would also like to thank Detlef Wilde and Uwe Bruege of Daimler-Chrysler Aerospace for their assistance and information concerning the X-Mir Inspector and ISS Inspector projects.

References

[1]Wilde, D., and Sytin, O., "The Mir-Progress-Inspector Mission," International Symposium Space Dynamics, Toulouse, France, 1995, MS95/020.

[2]"The Inspector Product Family," *DASA-RI Homepages*, URL: http://www.dasa.de/dasa/e/ri/orbit/insfam/insfam01.htm [cited 10 Feb. 2000].

[3]Choset, H., and Kortenkamp, D., "Path Planning and Control for Free-Flying Inspection Robot in Space," *ASCE Journal of Aerospace Engineering*, Vol. 12, No. 2, 1999, pp. 75–81.

[4]"AERCam Sprint," NASA Human Space Flight–International Space Station web pages, URL: http://www.shuttle.nasa.gov/station/index.html [cited 10 Feb. 2000].

[5]"Interface Definition Document for International Space Station Visiting Vehicles," International Space Station Program Office, NASA Johnson Space Center, Houston, TX, SPP 50235, 1988.

[6]St. John-Olcayto, E., and McInnes, C. R., "Applicability of Potential Function Method to Path Constrained Manoeuvre," European Space Research and Technology Centre, Contract 11478/95/NL/JQ/SC, 2200 AG Noordwijk, The Netherlands, Nov. 1997.

[7]McInnes, C. R., "Potential Function Methods for Autonomous Spacecraft Guidance and Control," American Astronautical Society Paper 95-447, Aug. 1995.

[8]Rimon, E., and Koditschek, D. E., "Exact Robot Navigation Using Artificial Potential Functions," *IEEE Transactions on Robotics and Automation*, Vol. 8, No. 5, 1992, pp. 501–518.

[9]Schmidt, G. K., and Azarm, K., "Mobile Robot Navigation in a Dynamic World Using an Unsteady Diffusion Equation Strategy," *Proceedings of the 1992 IEEE/RSJ International conference on Intelligent Robots and Systems*, IEEE Publications, Piscataway, NJ, 1992, pp. 642–647.

[10]Sato, K., "Deadlock-Free Motion Planning Using the Laplace Potential Field," *Advanced Robotics*, Vol. 7, No. 5, 1993, pp. 449–461.

[11]Akishita, S., Kawamura, S., and Hayashi, K., "Laplace Potential for Moving Obstacle Avoidance and Approach of a Mobile Robot," *Proceedings of 1990 Japan-USA Symposium on Flexible Automation*, Inst. of Systems, Control and Information Engineers of Japan and American Society of Mechanical Engineers, New York, pp. 139–142.

[12]Zelinsky, A., "A Mobile Robot Exploration Algorithm," *IEEE Transactions on Robotics and Automation*, Vol. 8, No. 6, 1992, pp. 707–717.

[13]Sallaberger, C. S., and D'Eleuterio, G. M. T., "Optimal Motion Planning for Space Robots," 43rd IAF Congress, International Astronautical Federation, Washington, DC, Aug.–Sept. 1992, IAF-92-0040.

[14]Leonard, C. L., Hollister, W. M., and Bergmann, E. V., "Orbital Formationkeeping with Differential Drag," *Journal of Guidance, Control, and Dynamics*, Vol. 12, No. 1, 1979, pp. 108–113.

[15]Clohessy, W. H., and Wiltshire, R. S., "Terminal Guidance System for Satellite Rendezvous" *Journal of the Aerospace Sciences*, Vol. 27, No. 9, 1960, pp. 653–658.

[16]"Mission and System Requirements Document," Daimler–Chrysler Aerospace, IINS-RIBRE_RQ-0001, 28059 Bremen, Germany, 1997.

[17]"Safety Requirements Document," International Space Station Program Office, NASA Johnson Space Center, Houston, TX, SPP 50021, 1988.

[18]Press, W. H., Teukolsky, S. A., Vetterling, W. T., and Flannery, B. P., "Interpolation in 2 or More Dimensions" *Numerical Recipes in C: The Art of Scientific Computing*, 2nd ed., Cambridge Univ. Press, Cambridge, England, U.K., 1992, pp. 123–125.